Structural insights into the π-π-π stacking mechanism and DNA-binding activity of the YEATS domain

Brianna J. Klein[1], Kendra R. Vann[1], Forest H. Andrews[1], Wesley W. Wang[2], Jibo Zhang[3], Yi Zhang[1], Anastasia A. Beloglazkina[4], Wenyi Mi[5], Yuanyuan Li[6], Haitao Li[6], Xiaobing Shi[5], Andrei G. Kutateladze[4], Brian D. Strahl[3], Wenshe R. Liu[2], and Tatiana G. Kutateladze[1]

[1]Department of Pharmacology, University of Colorado School of Medicine, Aurora, CO, 80045, USA

[2]Department of Chemistry, Texas A&M University, College Station, TX 77843, USA

[3]Department of Biochemistry & Biophysics, The University of North Carolina School of Medicine, Chapel Hill, NC 27599, USA

[4]Department of Chemistry and Biochemistry, University of Denver, Denver, CO 80210, USA

[5]Center for Epigenetics, Van Andel Research Institute, Grand Rapids, Michigan, 49503 USA

[6]Department of Basic Medical Sciences, School of Medicine, Tsinghua University, Beijing 100084, P.R. China

These authors contributed equally: Brianna J. Klein, Kendra R. Vann, Forest H. Andrews

Correspondence and requests for materials should be addressed to T.G.K. (email:tatiana.kutateladze@ucdenver.edu)

Abstract

The YEATS domain has been identified as a reader of histone acylation and more recently emerged as a promising anti-cancer therapeutic target. Here, we detail the structural mechanisms for π-π-π stacking involving the YEATS domains of yeast Taf14 and human AF9 and acylated histone H3 peptides and explore DNA-binding activities of these domains. Taf14-YEATS selects for crotonyllysine, forming π stacking with both the crotonyl amide and the alkene moiety, whereas AF9-YEATS exhibits comparable affinities to saturated and unsaturated acyllysines, engaging them through π stacking with the acyl amide. Importantly, AF9-YEATS is capable of binding to DNA, whereas Taf14-YEATS is not. Using a structure-guided approach, we engineered a mutant of Taf14-YEATS that engages crotonyllysine through the aromatic-aliphatic-aromatic π stacking and shows high selectivity for the crotonyl H3K9 modification. Our findings shed light on the molecular principles underlying recognition of acyllysine marks and reveal a previously unidentified DNA-binding activity of AF9-YEATS.

Introduction

A large number of epigenetic marks or posttranslational modifications (PTMs) in histones have been discovered over the past few years.[1,2] One of the major and widespread PTMs is acylation of the ε-amino group of lysine residues. Acylation neutralizes the positive charge and increases the hydrophobic character of the lysine side chain and alters chromatin structure utilizing two fundamental mechanisms. It weakens non-specific electrostatic interactions between histones and DNA, leading to a more open and transcriptionally active chromatin. It also recruits acyllysine readers and their host proteins and complexes to specific genomic loci to facilitate diverse epigenetic-driven nuclear programs essential in chromatin remodeling, gene transcription, and DNA replication, recombination and repair.[3,4] At least nine acyllysine modifications in histones have been identified, including crotonylation.

Since the discovery of lysine crotonylation in mammalian cells, this PTM has drawn much attention becoming an increasingly important epigenetic mark.[5,6] Crotonylation is enriched around active gene promoters and potentially enhancers and was found to stimulate gene transcription to a higher degree than the corresponding acetylation.[6] Studies of genomic distribution of crotonyllysine and acetyllysine reveal some differences, which suggest that these modifications are not redundant and can be associated with distinct biological outcomes.[5,6] Nevertheless, a substantial overlap in genomic localization and similarities in chemical properties present a challenge in studying and distinguishing the biological roles of these PTMs. A strategy of employing separate readers as probes for targeting individual acyllysine modifications has not been well developed, in part because of the promiscuous nature of currently known readers. Canonical acyllysine readers, bromodomain and double PHD finger (DPF), display comparable binding capabilities towards various short acyl chain modifications,[7-12] and while the YEATS domain exhibits preference for crotonyllysine, it still associates albeit more weakly with other acyllysine marks.[13-22] We have previously shown that the YEATS domains of Taf14 (Taf14-YEATS) and AF9 (AF9-YEATS) recognize crotonyllysine through a

non-canonical π-π-π stacking mechanism,[16,17] and in the case of Taf14-YEATS it involves aromatic-amide-aromatic π stacking and aromatic-aliphatic-aromatic π stacking[16] (Fig. 1a). In this study, we elucidate the significance of π stacking components in targeting of acetyllysines by the YEATS domains and report a previously uncharacterized DNA-binding activity of the human AF9 YEATS domain. We also show how the unique nature of the conjugated π system of the crotonyl modification could aid in the design of effectors indifferent to saturated acyllysines.

Results and Discussion

Structural insight into the selectivity of Taf14-YEATS

To determine the contribution of π stacking to the binding energetics, we measured binding affinities of Taf14-YEATS to the histone H3K9acyl peptides containing unsaturated and saturated four-carbon acyl modifications. Tryptophan fluorescence measurements showed that binding of Taf14-YEATS was reduced ~3-fold when the crotonylated modification was replaced with a similar in length but saturated butyryl modification (Fig. 1b, c and Supplementary Figure 1). The binding was further decreased to a negatively charged succinyllysine, and no interaction was detected with a branched hydroxyisobutyryllysine in $^{1}H,^{15}N$ heteronuclear single quantum coherence (HSQC) NMR titration experiments (Supplementary Figure 2). The selectivity of the YEATS domain for the crotonyllysine modification was substantiated by pull down assays with biotinylated histone peptides (Fig. 1d). GST fused Taf14-YEATS recognized the H3K9cr peptide but associated weaker with H3K9bu and H3K9ac peptides. Together these results demonstrate that Taf14-YEATS selects for unbranched acyl modifications, and the alkene group in the modification enhances the protein binding capability.

To gain insight into the molecular basis for the enhancement, we obtained the crystal structure of Taf14-YEATS in complex with H3K9bu peptide and compared it to the previously

reported structure of this domain in complex with H3K9cr.[16] The structures were superimposed with a root mean square deviation of 0.1 Å, indicating overall conservation of the binding mode. As in the case of crotonyllysine, butyryllysine transversed a narrow tunnel and was sandwiched between two aromatic residues of the protein, W81 and F62 (Fig. 1e, Supplementary Figure 3a and Supplementary Table 1). Amide nitrogen and carbonyl oxygen of butyryllysine were restrained through hydrogen bonds with the hydroxyl group of T61 and backbone amide of W81 and through a water-mediated hydrogen bond with G82. A similar set of polar interactions stabilized the complex with crotonyllysine, however substantial differences were observed in the position of W81. It adopted a single conformation, rotamer 1 (r1), involved in the π stacking interaction with butyryl amide in the Taf14 YEATS-H3K9bu complex. In contrast, when complexed with H3K9cr, W81 adopted two conformations, with r1 and r2 providing maximum π stacking with the crotonyl amide and the crotonyl alkene moiety, respectively (Supplementary Figures 3b and 4). Neither the complex with propionylated H3K9pr peptide nor the complex with acetylated H3K9ac peptide had the r2 conformation of W81, indicating that it is a unique feature available to the unsaturated acyl modification but not to saturated acyllysine modifications (Fig. 1f).

Design of the crotonyllysine specific Taf14-YEATS

Comparison of the H3K9bu- and H3K9cr-bound Taf14-YEATS structures revealed that the side chain of W81 is located within 4 Å of the α carbon atom of G82. Modeling in G82A mutation suggested that the presence of an additional methyl group at position 82 would hinder the ability of W81 to adopt the r1 conformation required for the π amide stacking. To test this hypothesis, we generated the G82A mutant of Taf14-YEATS and determined its crystal structure (Fig. 2a). In support of our idea, the indole moiety of W81 in this mutant was in a tilted conformation incompatible with r1 (Fig. 2b). We next assessed the acyllysine binding activity of Taf14-YEATS

G82A using NMR titration experiments (Fig. 2c). Large chemical shift perturbations (CSPs) in ^{15}N-labeled Taf14-YEATS G82A upon addition of H3K9cr peptide indicated that the mutant retains its ability to recognize the crotonyl modification. However, association of Taf14-YEATS with the H3K9ac peptide was almost negligible, as very small CSPs were observed (Fig. 2c and Supplementary Figure 5b). Tryptophan fluorescence measurements yielded a K_d of 124 μM for the interaction of Taf14-YEATS G82A with H3K9cr (Fig. 2d). Although binding affinity of the G82A mutant to H3K9cr was reduced compared to the binding affinity of the wild type protein, it remains in the range of affinities exhibited by the well-established readers of acetyllysine, bromodomains.[7,9]

We next characterized the Taf14-YEATS G82A mutant in the cellular context. We have previously shown that abrogating the Taf14 association with H3K9acyl through mutating W81 to alanine impacts the transcript levels of a variety of yeast genes both positively and negatively.[14] To determine the effect of blocking Taf14 from selectively associating with H3K9ac but not with H3K9cr, we carried out a real-time qPCR analysis for a set of Taf14-regulated genes in the *TAF14* deletion strain (*taf14Δ*) rescued with a vector only, wild-type *TAF14*, or with a form carrying either the W81A or G82A mutation in the YEATS domain (*taf14* W81A and *taf14* G82A) (Fig. 2e). As expected, *taf14Δ* deletion impacted the expression of multiple genes that were previously reported to be regulated by Taf14 interaction with H3K9acyl, including *YBL041, YPR145, YPR158, YER145C, YKL150W* and *YKR093W*.[14] For control, we also included several genes, such as *YLR290, YAL017* and *MRPL10*, that were shown not to be regulated by Taf14.[14] Intriguingly, while the effect of the entirely loss-of-function *taf14* W81A mutant was largely consistent with the effect seen with the loss of Taf14, the *taf14* G82A mutant showed more variable results (Fig. 2e). In some cases, the *taf14* G82A mutant impacted the expression of genes similar to that of the *taf14* W81A mutant (*YBL041, YPR158, YKL150W* and *YKR093W*), while in other cases, the *taf14* G82A mutant showed distinct effects on gene transcripts not seen in either the *taf14* W81A mutant or the *TAF14* deletion (*YPR145* and *YER145C*). Given

the *taf14* G82A mutation impacts H3K9ac binding to a greater degree than H3K9cr binding, these findings suggest a differential requirement of H3K9ac and H3K9cr for the proper expression of Taf14-regulated genes.

Crotonyllysine recognition by Taf14-YEATS G82A

To elucidate the mechanism by which Taf14-YEATS G82A distinguishes crotonyllysine and discriminates against saturated counterparts, we obtained the crystal structure of the H3K9cr-bound G82A mutant (Fig. 3a). The structure of the complex showed that the aromatic side chains of W81 and F62 lay parallel to each other and at equal distance of 3.4-3.6 Å from the crotonyl alkene group (Fig. 3b). Remarkably, only a single r2 conformation of W81 was observed in the structure of the complex. Analysis of molecular orbitals for the W81, Kcr and F62 assembly at the B3LYP/6-311+G(d,p) level of DFT (density functional theory) revealed that the bonding molecular orbitals (MOs) transcending all three π systems are deeply buried, indicating considerable synergism of the π-π-π stacking interaction (Supplementary Figure 6). A representative MO, the highest occupied molecular orbital HOMO-8, is shown in Figure 3c. We concluded that the ability of the W81 r2 rotamer to engage the crotonyl alkene moiety most likely accounts for the selectivity of Taf14-YEATS G82A.

AF9-YEATS is a more versatile acyllysine reader

Alignment of the YEATS domain sequences derived from the family of human and yeast proteins shows conservation of the WG motif (W81 and G82 in Taf14) in all YEATS members but AF9 and ENL, which instead contain a YA motif (Fig. 4a). Interestingly, despite the presence of an alanine following the aromatic Y78 residue in AF9, the YEATS domain of AF9 did not differentiate between acylated modifications on H3K9 and bound almost equally well to H3K9cr, H3K9bu and H3K9ac, supporting the original findings[17] (Fig. 4b and Supplementary Figure 7).

To compare the binding modes of the YEATS domains harboring the WG and YA motifs, we determined the structure of AF9-YEATS in complex with H3K9bu peptide. Structural overlay of the AF9-YEATS:H3K9bu and previously reported AF9-YEATS:H3K9cr[17] complexes showed that both saturated and unsaturated four-carbon acyl chains of K9 are bound by the three aromatic residues Y78, F59 and F28 in a very similar way (Fig. 4c). Short (less than 4 Å) distances observed between C^{γ}, C^{δ}, C^{ε}, and C^{η} atoms of Y78, the amide group of acyllysine, and the C^{ε} and C^{ζ} atoms of F59 indicated that Y78 and F59 of AF9 are involved in the aromatic-amide-aromatic π-π-π stacking in either complex (Fig. 4c, yellow dashed lines). However, neither Y78 nor F28 appear to form π-π-π stacking with the alkene group of crotonyllysine as only a single carbon atom in Y78 (C^{ε}) or F28 (C^{ε}) was close enough to the C=C carbon atoms to fully engage the double bond (Fig. 4c, red dashed lines). This inability to form the additional energetically favorable contact is likely the reason behind the indifference of the YEATS domain of AF9 toward crotonyl-, butyryl-, and acetyl- H3K9acyl modifications.

We next explored the possibility of engineering an AF9-based acyllysine specific reader through mutating Y78 in AF9-YEATS to a tryptophan and therefore re-creating the WA motif seen in the Taf14-YEATS G82A mutant. Although NMR titration experiments revealed a tight interaction of AF9-YEATS Y78W with H3K9cr, binding affinities measured by fluorescence spectroscopy indicated that this mutant does not differentiate between H3K9cr and H3K9ac and associates with both peptides with a K_d of 2 μM (Fig. 4b, d and e and Supplementary Figure 8a). To explain the different behavior of Taf14-YEATS G82A and AF9-YEATS Y78W, we obtained the crystal structure of AF9-YEATS Y78W in complex with H3K9cr peptide (Fig. 4f). In this complex, W78 was in a single r1 conformation, which was engaged in π stacking with the crotonyl amide. Notably, A79 imposed steric hindrance on W78 to a higher degree than on wild type Y78 at this position, resulting in a tilted conformation of W78 (Supplementary Figure 8b). W78 is incapable of adopting the r2 conformation necessary for π stacking with the alkene

group most likely because of steric hindrance from F28 (Supplementary Figure 8c). Additional mutation of A79 to a glycine in AF9, to recapitulate the Taf14' WG motif, failed to induce the selectivity as the AF9-YEATS Y78WA79G mutant bound equally well to either H3K9cr or H3K9ac peptide (Fig. 5a). By contrast, the W81Y mutant of Taf14-YEATS retained its capability to select for H3K9cr, suggesting that position of the tyrosine residue in this mutant allowed for π stacking with the alkene group (Fig. 5a and Supplementary Figure 9).

AF9-YEATS binds to DNA

Analysis of electrostatic surface potential of AF9-YEATS reveals that the part of the domain opposite to the H3K9cr-binding site is highly positively charged. Particularly, two apparent clusters of basic residues on the protein surface suggest that they could be involved in binding to negatively charged DNA (Fig. 5b). To determine whether AF9-YEATS is capable of interacting with DNA, we examined association of AF9-YEATS with 147 bp 601 Widom DNA using an electrophoretic mobility shift assay (EMSA). 601 DNA was incubated with increasing amounts of AF9-YEATS and the reaction mixtures were resolved on native polyacrylamide gels (Fig. 5c). A gradual increase in the amount of added AF9-YEATS resulted in a shift and disappearance of the 601 DNA band and the appearance of the bands corresponding to multiple complexes formed between AF9-YEATS and multiple major/minor grooves[23] of 601 DNA (Fig. 5c). Direct binding to DNA was corroborated by NMR titration experiments, in which substantial CSPs were observed in ^{15}N-labeled AF9-YEATS upon gradual addition of 601 DNA (Fig. 5d and Supplementary Figure 10a, b).

To assess how AF9-YEATS interacts with both H3K9acyl and DNA, we reconstituted H3K9acyl-containing nucleosome core particles (H3K9cr-NCPs and H3K9ac-NCP) and examined binding of AF9-YEATS to these NCPs and to unmodified NCP in EMSA. Incubation of increasing amounts of AF9-YEATS with H3K9cr-NCP led to a disappearance of the H3K9cr-NCP band and of free 601 DNA present in the sample, indicating formation of the AF9-

YEATS:H3K9cr-NCP and AF9-YEATS:601 DNA, respectively, complexes (Fig. 5e). We note that the free 601 DNA band disappeared faster than the H3K9cr-NCP band, implying that AF9-YEATS prefers a more accessible, free DNA to the DNA wrapped around the nucleosome, despite the fact that H3K9cr-NCP contains the additional binding partner of the YEATS domain – H3K9cr. Yet, the recognition of H3K9cr by the YEATS domain is required for strong interaction, as the AF9-YEATS association with unmodified NCP was substantially compromised (Fig. 5f) and its association with H3K9ac-NCP was slightly diminished (Supplementary Figure 10c). In further support, the H3K9cr-NCP binding capability of the AF9-YEATS F59A/Y78A mutant, which is defective in H3K9acyl binding,[22] was also markedly decreased (Fig. 5g).

DNA- and H3K9cr- binding sites in AF9-YEATS do not overlap

To map the DNA-binding site of AF9-YEATS, we plotted NMR CSPs induced in each amide of ^{15}N-labeled AF9-YEATS by 601 DNA and compared to CSPs induced in this protein by the H3K9cr peptide (Fig. 6a, b). Notably, residues located in and around the H3K9cr-binding site, including Y78, were most perturbed upon addition of the H3K9cr peptide (Fig. 6a, c). However, an entirely different set of residues was perturbed due to binding of 601 DNA (Fig. 6b, c). The most pronounced changes were observed in the residues located in three AF9-YEATS regions, i.e. the 60th, 90th and 130th patches (Fig. 6c, d). These patches contain the surface exposed positively charged R61, K63, R64, K67, K92, R96, K97, R133, K134 and K137 residues that can be directly or indirectly involved in electrostatic interactions with negatively charged 601 DNA.

To determine the contribution of the perturbed patches to DNA binding, we generated four mutants of AF9-YEATS, including R61E/K63E/K67E, K92E/R96E/K97E, R96E/K97E and R133E/K134E/K137E. Among them, only the R61E/K63E/K67E (thereafter referred to as RKK) mutant was soluble and folded. Binding of the AF9-YEATS RKK mutant to 601 DNA and H3K9cr-NCP was examined by EMSA. As shown in Figures 6e-g, the DNA-binding and H3K9cr-

NCP-binding abilities of this mutant were markedly reduced compared to the respective binding abilities of WT AF9-YEATS, pointing to a critical role of the 60th patch residues of AF9-YEATS in the interaction with DNA (Fig. 6c). Taken together, the EMSA results and NMR CSPs indicate that the 60th patch residues are part of the DNA-binding site of AF9-YEATS. A lack of mutually perturbed residues due to the interaction with H3K9cr peptide or 601 DNA further suggests that the H3K9cr- and DNA-binding sites of AF9-YEATS do not overlap.

Bivalent association of AF9 is not conserved in Taf14-YEATS

To identify the DNA fragments smaller than 147 bp of 601 DNA that can be bound by AF9-YEATS, we carried out EMSA assays with 20 bp DNA and 15 bp DNA (Fig. 7a and Supplementary Figure 11a). Both 15- and 20-mer DNA bands disappeared in an AF9-YEATS concentration dependent manner, and quantitative analysis of the band intensities yielded K_ds of 47 μM and 57 μM for 15-mer DNA and 20-mer DNA, respectively (Fig. 7b), which is in the range of DNA-binding affinities of other transcriptional regulators.[24] Overall, these and the results described above suggest that AF9-YEATS interacts with chromatin in a bivalent manner, i.e. it binds both H3K9acyl and DNA (Fig. 7c).

Is the bivalent interaction conserved in other YEATS domains? Alignment of the YEATS sequences reveals that all three positively charged patches are conserved in the YEATS domain of another human protein, ENL, and thus ENL-YEATS is likely capable of binding to DNA (Fig. 7d). Although these patches are not strictly conserved in the YEATS domain of the human protein YEATS2, the “DNA-binding” surface in YEATS2-YEATS is also highly positively charged (Supplementary Figure 11b). Altogether, these observations suggest that the DNA-binding function may be conserved in the family of human YEATS readers. In contrast, the corresponding Taf14-YEATS surface is enriched in the negatively charged residues that can electrostatically repulse DNA (Fig. 7e). Indeed, EMSA experiment using 601 DNA showed that even a large, up to ~10^3-fold, excess of Taf14-YEATS failed to shift the DNA band, implying that

this domain does not bind DNA (Fig. 7f). Interestingly, similar to Taf14-YEATS, the YEATS domain of another yeast protein, Yaf9, also has a negatively charged and therefore repulsive of DNA surface opposite to its H3K27acyl-binding site, which may indicate that the ability to interact with DNA is lost in yeast YEATS domains (Supplementary Figure 11b).

Collectively, our results have illuminated the mechanistic basis underlying distinct recognition of acyllysine PTMs by the YEATS domains of yeast Taf14 and human AF9, allowing us to develop a Taf14-YEATS module that selects for the crotonyl modification and discriminates against saturated acyl modifications. The discovery of the DNA-binding function for AF9-YEATS expands the family of epigenetic readers capable of bivalently interacting with histone tails and nucleosomal DNA. These include the Tudor domain of PHF1[25,26], the PWWP domains of LEDGF and PSIP1[27,28], the PZP domain of BRPF1[29], and bromodomain of BRDT[30]. It will be interesting in future studies to explore the idea of conservation of DNA-binding activities in YEATS readers derived from different organisms.

Methods

Protein expression and purification

The Taf14 YEATS domain (aa 1-132 and 1–137) in a pGEX-6P1 vector and the AF9 YEATS domain (aa 1–138) in a pET28b vector were used in this study.[13,16] The YEATS domain mutants of Taf14 (W81Y and G82A) and AF9 (Y78W, Y78W/A79G, R61E/K63E/K67E, K92E/R96E/K97E, R96E/K97E, and R133E/K134E/K137E) were generated using standard QuikChange site-directed mutagenesis protocols (Stratagene) (Supplementary Figure 12). Wild type and mutant proteins were expressed in *E. coli* BL21 (DE3) RIL (Agilent) cells grown in either Luria Broth or M9 minimal media supplemented with $^{15}NH_4Cl$ (Sigma-Aldrich). Following induction with IPTG, cells were harvested by centrifugation and lysed by sonication. 25 mM Tris pH 7.5 buffer, supplemented with 500 mM NaCl, 2 mM β-mercaptoethanol, 1% Triton X-100, and DNase I was used for AF9-YEATS, and 50 mM HEPES pH 7.5 buffer, supplemented with

150 mM NaCl, 1 mM TCEP, and 0.1% Triton X-100 was used for Taf14-YEATS. GST-fusion proteins were purified on glutathione Sepharose 4B beads (Thermo Fisher), and the GST tag was either cleaved with PreScission protease overnight, or left on and the proteins then were eluted off the resin with 50 mM reduced L-glutathione (Fisher). His tag fusion proteins were purified on a nickel–NTA resin (Qiagen), and the His tag was cleaved with Thrombin. Proteins were further purified by size exclusion chromatography using a S100 column or Hi- Trap SP HP and HiPrep 16/600 Superdex 75 columns (GE Healthcare). The proteins were concentrated in Millipore concentrators and stored at -80°C.

X-ray data collection and structure determination

Taf14-YEATS proteins (1-137) were buffer exchanged and concentrated to 14 mg/mL in 50 mM MES (pH 6.5) at 4 °C. Wild type Taf14-YEATS was incubated with 5 molar equivalents of either H3K9bu (5-13) or H3K9pr (5-13) peptide at 25 °C for 30 min prior to crystallization. Crystals were obtained by the sitting drop vapor diffusion method at 18 °C. The 1.6 µl crystallization drop contained a 1:1 ratio of protein–ligand solution to reservoir solution composed of 44-46% PEG 600 (*v*/*v*) and 0.2 M citric acid pH 6.0. Taf14-YEATS G82A was incubated with 10 molar equivalents of the H3K9cr (5-13) and crystallized under the same conditions as wild type Taf14-YEATS. The mutant in the apo- state was crystallized in a 1:1 ratio with a reservoir solution composed of 48% PEG 600 (*v*/*v*) and 0.2 M sodium citrate pH 6.0. X-ray diffraction data were collected at a wavelength of 1.0 or 1.54 Å and a temperature of 100 K on a Rigaku Micromax 007 high-frequency microfocus X-ray generator with a Pilatus 200K 2D area detector at the UC Denver Biophysical Core facility or on beamline 4.2.2 at the Advance Light Source administrated by the Molecular Biology Consortium.

The AF9-YEATS proteins, Y78W mutant and wild type, were buffer exchanged and concentrated at 4 °C in 50 mM sodium citrate pH 6.5, 5 mM DTT, or 50 mM Bis-Tris pH 6.5, 5 mM DTT, respectively. AF9-YEATS Y78W was incubated at 6 mg/ml with a 2-molar equivalence

of H3K9cr (5-14) peptide at RT for 30 min before crystallization. Crystals of AF9-YEATS Y78W in complex with H3K9cr were grown at 4 °C, using the sitting-drop vapor diffusion method against 100 mM MES pH 6.0, 20%(w/v) PEG 6000, and 10 mM $ZnCl_2$ reservoir solution. The 1.0 µl crystallization drop contained a 1:1 ratio of protein-ligand to reservoir solution. Crystals were cryoprotected with 25% (v/v) glycerol. Wild type AF9-YEATS was incubated at 6 mg/ml with a 2-molar equivalence of H3K9bu (1-19). Crystals were grown at 4 °C, using the sitting-drop vapor diffusion method in a 1:1 ratio of protein-ligand to reservoir solution (200 mM sodium malonate, 100 mM Bis-Tris propane pH 8.5, and 20% (w/v) PEG 3350) in a 1.0 µl crystallization drop and were cryoprotected with 25% (v/v) glycerol. X-ray diffraction data from AF9-YEATS Y78W:H3K9cr and AF9-YEATS:H3K9bu crystals were collected at a wavelength of 1.28 and 0.98 Å, respectively, and a temperature of 100 K on beamline 4.2.2 at the Advance Light Source administrated by the Molecular Biology Consortium.

HKL3000 was used for indexing, scaling, and data reduction.[31] The phase solutions were solved by molecular replacement with Phaser using a modified Taf14 or AF9 YEATS domain as a search model (PDB 5D7E and 4TMP, respectively). Model building was carried out with Coot and refinement was performed with Phenix.Refine.[32,33] Coot and Molprobity were used to verify the model fit to density and model quality.[32,34] The crystallographic and refinement statistics are shown in Supplementary Table 1.

NMR spectroscopy

NMR experiments were performed at 298 K on a Varian INOVA 600 MHz spectrometer equipped with a cryogenic probe. $^{1}H,^{15}N$ HSQC spectra of 0.1-0.2 mM uniformly ^{15}N-labeled wild type or mutated Taf14-YEATS (in PBS buffer pH 6.8, 8% D_2O) and AF9-YEATS (in 25 mM Tris-HCl pH 7.5, 250 mM NaCl, 2 mM BME, 8-10% D_2O) were recorded in the presence of increasing concentrations of H3K9cr, H3K9bu, H3K9ac, H3K9su, or H3K9hib peptides. K_d value was calculated by a nonlinear least-squares analysis in Kaleidagraph using the equation:

$$\Delta\delta = \Delta\delta_{max}\frac{\left(([L]+[P]+K_d)-\sqrt{([L]+[P]+K_d)^2-4[P][L]}\right)}{2[P]} \quad (1)$$

where [L] is concentration of free acetyllysine, [P] is concentration of the protein, Δδ is the observed chemical shift change, and $\Delta\delta_{max}$ is the normalized chemical shift change at saturation. Normalized chemical shift changes were calculated using the equation

$$\Delta\delta = \sqrt{(\Delta\delta H)^2 + \left(\frac{\Delta\delta N}{5}\right)^2} \quad (2)$$

where Δδ is the change in chemical shift in parts per million (ppm).

Fluorescence spectroscopy

Spectra were recorded at 25 ˚C on a Fluoromax-3 spectrofluorometer (HORIBA). The samples containing 1-2 μM wild-type or mutated YEATS domains in PBS buffer pH 7.4 (Taf14) or 20 mM Tris pH 7.5, 500 mM NaCl, and 2 mM BME (AF9) and progressively increasing concentrations of H3 peptides, H3K9cr, H3K9ac, or H3K9bu (all aa 5-13) (Synpeptide) were excited at 295 or 280 nm. Emission spectra were recorded between 300 and 380 nm with a 1 nm step size and a 0.5 s integration time. K_d values were determined using a nonlinear least-squares analysis and the equation:

$$\Delta\mathrm{I} = \Delta\mathrm{I}_{max}\frac{\left(([L]+[P]+K_d)-\sqrt{([L]+[P]+K_d)^2-4[P][L]}\right)}{2[P]} \quad (3)$$

where [L] is the concentration of the histone peptide, [P] is the concentration of the protein, ΔI is the observed change of signal intensity, and ΔI_{max} is the difference in signal intensity of the free and bound states of the protein. K_d values were averaged over three separate experiments, and error was calculated as the standard deviation between the runs.

Real Time-qPCR

Real Time-qPCR was performed essentially as described.[35] Briefly, wild-type or *taf14* mutant yeast cells were cultured in YPD overnight at 30˚C and cell pellets corresponding to 10 OD_{600}

equivalents were collected. Total RNA was extracted using the phenol/chloroform method as described[35] and RNA was treated with DNase I to eliminate residual DNA. 2 mg of RNA was used to produce cDNA with random hexamer primers and reverse transcriptase IScript (BioRad). cDNA was diluted to 0.1 mg/ml and SYBR green master mix was used for real-time qPCR. *ACT1* was also examined and used as a normalization control. The expression of all Taf14 proteins were equal in abundance, indicating that the expression effects observed are due to Taf14 acyl-lysine binding defects. The data shown are from three biological replicates.

Expression and Purification of H3 mutants H3K9ac and H3K9cr

To incorporate N-ε-acetyl-L-lysine (AcK) into the K9 position of histone H3, pETDuet-1 vector encoding human histone H3 with amber stop codon (pETDuet-1-H3K9TAG) introduced at H3K9 was used to co-transform E. coli BL21 (DE3)-ΔcobB strain with pEVOL-MmAcKRS. Single colony was picked and inoculated in 2YT medium supplemented with 100mg/L ampicillin and 34 mg/L chloramphenicol. When OD reached to 0.6, H3 expression was induced at 37℃ by adding 0.5 mM IPTG, 0.2% (w/v) L-arabinose and 5 mM AcK into cell culture. Cells were harvested 6 hours after induction, and purified in the same steps as previously reported.[36] The whole procedure of CrK (N-ε-crotonyl-L-lysine) incorporation into the K9 position of histone H3 was identical with AcK incorporation, except that pEVOL-MmPylRS-384W vector was used, and 1mM of CrK (N-ε-crotonyl-L-lysine) was added into 2YT medium after induction.

Assembly of nucleosomes

Recombinant Histone His-TEV-H2A, His-TEV-H2B and His-SUMO-TEV-H4 were purified in the previously reported steps.[36] All 4 histone pellets including histone H3K9ac or H3K9cr were dissolved in 6 M GuHCl buffer (6 M guanidinium hydrochloride, 20 mM Tris, 500 mM NaCl, pH 7.5), and concentration was measured by UV absorption at 280 nm (Biotek synergy H1 plate reader). To prepare H2A/H2B dimer, His-TEV-H2A and His-TEV-H2B were mixed in the molar

ratio of 1:1, and 6 M GuHCl buffer was added to adjust total protein concentration to 4 μg/μl. Denatured His-TEV-H2A/His-TEV-H2B solution was dialyzed sequentially at 4℃ against 2 M TE buffer (2 M NaCl, 20 mM Tris, 1 mM EDTA, pH 7.8), 1M TE buffer (1 M NaCl, 20 mM Tris, 1 mM EDTA), 0.5 M TE buffer (0.5 M NaCl, 20 mM Tris, 1 mM EDTA). Then the resulting dimer solution was centrifuged for 5 min at 4℃ to remove precipitates, and the concentration of dimer was determined by UV absorption at 280 nm. Steps of His-TEV-H3/His-SUMO-TEV-H4 tetramer refolding were generally the same as His-TEV-H2A/His-TEV-H2B dimers except that the total protein concentration should be adjusted to 2 μg/μl and no stirring in the sequential dialysis. Then His-TEV-H2A/Hi-TEV-H2B dimers were mixed with His-TEV-H3/His-SUMO-TEV-H4 tetramers in a molar ratio of 1:1 to generate histone octamers, and NaCl solid was added to adjust NaCl concentration to 2 M. The 147 bp biotinylated 601 nucleosome positioning was prepared by Polymerase chain reaction with biotinylated primers and purified with PCR cleanup kit (#2360250 Epoch Life Science). Purified 147 bp DNA was re-dissolved in 2 M TE buffer and added to histone octamer solution in the molar ratio of 0.85:1. 2 M TE buffer was added to adjust final 147 bp DNA concentration to 2-3 μM. The DNA histone mixture solution was then transferred to a dialysis bag and placed inside about 200 ml 2 M TE buffer, while stirring at room temperature, Tris buffer with no salt (20 mM Tris) was slowly added into the 2 M salt buffer through a liquid transfer pump (#23609-170 VWR®). Nucleosomes formed when salt concentration was reduced to around 150 mM (measured by EX170 salinity meter), and the DNA histone mixture solution was further dialyzed into low salt Tris buffer (20 mM Tris, 20 mM NaCl, 0.5 mM EDTA, pH 7.8). Precipitates were removed by centrifuge, and the concentration of the nucleosomes was measured by A260 reading using the Biotek synergy H1 plate reader. His-TEV protease was added to nucleosome solutions (TEV:nucleosome 1:30, w:w) to remove all the histone tags after incubation for 1 hour at 37℃, and finally all the His tagged impurities were removed from nucleosome solution by Ni^{2+}-NTA resin (Thermo Fisher #88221).

Peptide pulldown assays

1 µg of biotinylated histone peptides with different modifications were incubated with 1–2 µg of GST-fused proteins in binding buffer (50 mM Tris-HCl 7.5, 150 mM NaCl, 0.1% NP-40, 1 mM PMSF) overnight. Streptavidin beads (Amersham) were added to the mixture, and the mixture was incubated for 1 h with rotation. The beads were then washed three times and analyzed using SDS–PAGE and western blotting. Anti-GST (sc-459, 1:1000) antibody was from Santa Cruz (Supplementary Figure 13).

MOs computations

All computations were performed on a Linux HPC cluster with the Gaussian 09 quantum chemical software package (Gaussian 09, Revision A.02, M. J. Frisch et al., Gaussian, Inc., Wallingford CT, 2016). X-ray coordinates of the carbon, oxygen, and nitrogen atoms belonging to the triple-stacked truncated trp – crotonamide – phe fragment were frozen, while the positions of the attached hydrogen atoms were fully optimized at the B3LYP/6-311+G(d,p) level of DFT theory producing the truncated structure (Supplementary Figure 6). XYZ coordinates for the truncated triple-stack structure with fully optimized hydrogens are available upon request.

Electrophoretic mobility shift assay

A total of 32 repeats of the 601 Widom DNA sequence were cloned into the pJ201 plasmid and transformed into DH5α cells. The plasmid was purified as previously described [25]and by Qiagen-QIAprep Spin Miniprep kit. Separation of the individual sequences was completed by digestion of the plasmid with EcoRV. The 601 Widom DNA was purified from the remaining plasmid by gel extraction (Qiagen-MinElute Gel Extraction kit). Annealed DNA was made up of single stranded oligos (IDT) in water brought up to 95°C for 20 minutes then cooled to 16 at 0.1°C/second. Increasing amounts of the Taf14 and AF9 YEATS domains were incubated with

601 Widom DNA (1-3 pmol/lane), annealed double stranded DNA in buffer (20 mM Tris-HCl pH 7.5 and 150 mM NaCl), or nucleosome in buffer (20 mM Tris-HCl pH 7.5,150 mM NaCl, 0.1 mM EDTA, and 10% glycerol) for 30 minutes at room temperature. Specifically, for each lane, 1.88 pmol (Figs. 5c, 7f) or 1 pmol (Fig. 6e, f) 601 DNA, 5 pmol 20-mer DNA (Fig. 7a), or 5 pmol 15-mer DNA (Supplementary Figure 11a) was incubated with increasing amounts of mutant or wild type AF9-YEATS or Taf14-YEATS. 1 pmol/lane (Figs. 5e-g and 6g and Supplementary Figure 10c) of nucleosome was incubated with increasing wild type or mutant AF9-YEATS domain. The reaction mixtures were loaded on 5-10% native polyacrylamide gels and electrophoresis was performed in 0.2× TB or TBE buffer (1× TB/TBE = 90 mM Tris, 64.6 mM boric acid, with or without 2 mM EDTA) at 100–130 V on ice. Gels were stained with ethidium bromide or SYBR Gold (ThermoFisher) and visualized at 365mm or by Blue LED (UltraThin LED Illuminator-GelCompany). Quantification of gel bands was performed using ImageJ. Each EMSA experiment was performed five times (Figs. 5c and 6e), four times (Figs. 7a, f and Supplementary Figure 11a), three times (Fig. 5e), twice (Fig. 5f and Supplementary Figure 10c), and once (Figs. 5g and 6f, g).

Data availability

The atomic coordinates and structure factors of Taf14-YEATS and AF9-YEATS have been deposited in the Protein Data Bank under the accession codes 6MIQ, 6MIP, 6MIO, 6MIN, 6MIM, 6MIL. Other data are available from the corresponding author upon reasonable request.

References

1 Huang, H., Sabari, B. R., Garcia, B. A., Allis, C. D. & Zhao, Y. M. SnapShot: Histone Modifications. *Cell* **159**, 458-+, (2014).

2 Huang, H., Lin, S., Garcia, B. A. & Zhao, Y. Quantitative proteomic analysis of histone modifications. *Chemical reviews* **115**, 2376-2418, (2015).

3 Musselman, C. A., Lalonde, M. E., Cote, J. & Kutateladze, T. G. Perceiving the epigenetic landscape through histone readers. *Nature structural & molecular biology* **19**, 1218-1227, (2012).

4 Andrews, F. H., Strahl, B. D. & Kutateladze, T. G. Insights into newly discovered marks and readers of epigenetic information. *Nature chemical biology* **12**, 662-668, (2016).

5 Tan, M. *et al.* Identification of 67 histone marks and histone lysine crotonylation as a new type of histone modification. *Cell* **146**, 1016-1028, (2011).

6 Sabari, B. R. *et al.* Intracellular Crotonyl-CoA Stimulates Transcription through p300-Catalyzed Histone Crotonylation. *Molecular cell* **58**, 203-215, (2015).

7 Dhalluin, C. *et al.* Structure and ligand of a histone acetyltransferase bromodomain. *Nature* **399**, 491-496, (1999).

8 Zeng, L. *et al.* Mechanism and regulation of acetylated histone binding by the tandem PHD finger of DPF3b. *Nature* **466**, 258-262, (2010).

9 Filippakopoulos, P. *et al.* Histone recognition and large-scale structural analysis of the human bromodomain family. *Cell* **149**, 214-231, (2012).

10 Ali, M. *et al.* Tandem PHD fingers of MORF/MOZ acetyltransferases display selectivity for acetylated histone H3 and are required for the association with chromatin. *Journal of molecular biology* **424**, 328-338, (2012).

11 Klein, B. J. *et al.* Recognition of Histone H3K14 Acylation by MORF. *Structure* **25**, 650-654 e652, (2017).

12 Dreveny, I. *et al.* The double PHD finger domain of MOZ/MYST3 induces alpha-helical structure of the histone H3 tail to facilitate acetylation and methylation sampling and modification. *Nucleic acids research* **42**, 822-835, (2014).

13 Li, Y. *et al.* AF9 YEATS domain links histone acetylation to DOT1L-mediated H3K79 methylation. *Cell* **159**, 558-571, (2014).

14 Shanle, E. K. *et al.* Association of Taf14 with acetylated histone H3 directs gene transcription and the DNA damage response. *Genes Dev* **29**, 1795-1800, (2015).

15 Andrews, F. H., Shanle, E. K., Strahl, B. D. & Kutateladze, T. G. The essential role of acetyllysine binding by the YEATS domain in transcriptional regulation. *Transcription* **7**, 14-20, (2016).

16 Andrews, F. H. *et al.* The Taf14 YEATS domain is a reader of histone crotonylation. *Nature chemical biology* **12**, 396-U333, (2016).

17 Li, Y. *et al.* Molecular Coupling of Histone Crotonylation and Active Transcription by AF9 YEATS Domain. *Molecular cell* **62**, 181-193, (2016).

18 Erb, M. A. *et al.* Transcription control by the ENL YEATS domain in acute leukaemia. *Nature* **543**, 270-274, (2017).

19 Wan, L. *et al.* ENL links histone acetylation to oncogenic gene expression in acute myeloid leukaemia. *Nature* **543**, 265-269, (2017).

20 Zhao, D. *et al.* YEATS2 is a selective histone crotonylation reader. *Cell Research* **26**, 629-632, (2016).

21 Klein, B. J. *et al.* Yaf9 subunit of the NuA4 and SWR1 complexes targets histone H3K27ac through its YEATS domain. *Nucleic acids research* **46**, 421-430, (2018).

22 Zhang, Q. *et al.* Structural Insights into Histone Crotonyl-Lysine Recognition by the AF9 YEATS Domain. *Structure* **24**, 1606-1612, (2016).

23 Davey, C. A., Sargent, D. F., Luger, K., Maeder, A. W. & Richmond, T. J. Solvent mediated interactions in the structure of the nucleosome core particle at 1.9 a resolution. *Journal of molecular biology* **319**, 1097-1113, (2002).
24 Schlundt, A. *et al.* Structure-function analysis of the DNA-binding domain of a transmembrane transcriptional activator. *Scientific reports* **7**, 1051, (2017).
25 Musselman, C. A. *et al.* Binding of PHF1 Tudor to H3K36me3 enhances nucleosome accessibility. *Nature communications* **4**, 2969, (2013).
26 Gibson, M. D., Gatchalian, J., Slater, A., Kutateladze, T. G. & Poirier, M. G. PHF1 Tudor and N-terminal domains synergistically target partially unwrapped nucleosomes to increase DNA accessibility. *Nucleic acids research*, (2017).
27 Eidahl, J. O. *et al.* Structural basis for high-affinity binding of LEDGF PWWP to mononucleosomes. *Nucleic acids research* **41**, 3924-3936, (2013).
28 van Nuland, R. *et al.* Nucleosomal DNA binding drives the recognition of H3K36-methylated nucleosomes by the PSIP1-PWWP domain. *Epigenetics & chromatin* **6**, 12, (2013).
29 Klein, B. J. *et al.* Bivalent interaction of the PZP domain of BRPF1 with the nucleosome impacts chromatin dynamics and acetylation. *Nucleic acids research* **44**, 472-484, (2016).
30 Miller, T. C. *et al.* A bromodomain-DNA interaction facilitates acetylation-dependent bivalent nucleosome recognition by the BET protein BRDT. *Nature communications* **7**, 13855, (2016).
31 Minor, W., Cymborowski, M., Otwinowski, Z. & Chruszcz, M. HKL-3000: the integration of data reduction and structure solution--from diffraction images to an initial model in minutes. *Acta crystallographica. Section D, Biological crystallography* **62**, 859-866, (2006).
32 Emsley, P., Lohkamp, B., Scott, W. G. & Cowtan, K. Features and development of Coot. *Acta crystallographica. Section D, Biological crystallography* **66**, 486-501, (2010).
33 Adams, P. D. *et al.* PHENIX: a comprehensive Python-based system for macromolecular structure solution. *Acta crystallographica. Section D, Biological crystallography* **66**, 213-221, (2010).
34 Chen, V. B. *et al.* MolProbity: all-atom structure validation for macromolecular crystallography. *Acta crystallographica. Section D, Biological crystallography* **66**, 12-21, (2010).
35 Dronamraju, R. *et al.* Spt6 Association with RNA Polymerase II Directs mRNA Turnover During Transcription. *Molecular cell* **70**, 1054-1066 e1054, (2018).
36 Wang, W. W., Zeng, Y., Wu, B., Deiters, A. & Liu, W. R. A Chemical Biology Approach to Reveal Sirt6-targeted Histone H3 Sites in Nucleosomes. *ACS chemical biology* **11**, 1973-1981, (2016).

Acknowledgements

We thank Jinyong Zhang, Ruben Rosas-Ospina and Jayce Breig for help with experiments, Jay Nix at beam line 4.2.2 of the ALS in Berkeley for help with X-ray crystallographic data collection, and Ming-Ming Zhou for a kind gift of cDNA of the AF9-YEATS F59A/Y78A mutant. This work was supported in part by grants from NIH GM106416, GM100907 and GM125195 to T.G.K.,

GM121584 to W.R.L., R35GM126900 to B.D.S., and CA204020 to X.S., and from NSF CHE-1665342 to A.G.K. X.S. is a Leukemia & Lymphoma Society Career Development Program Scholar (1339-17).

Author contributions

B.J.K., K.R.V., F.H.A., W.W.W., J.Z., Y.Z., A.A.B., W.M., and Y.L. performed experiments and together with H.L., X.S., A.G.K., B.D.S., W.R.L. and T.G.K. analyzed the data. B.J.K., K.R.V., F.H.A. and T.G.K. wrote the manuscript with input from all authors.

Competing Interests

The authors declare no competing interests.

Figure legends

Figure 1. Structural insight into the selectivity of Taf14-YEATS. (a) Crotonylated lysine (yellow) is sandwiched between W81 and F62 in the complex of Taf14-YEATS with H3K9cr. W81 adopts two conformations, rotamer 1 (light gray) and rotamer 2 (green). (b) Binding affinities of Taf14-YEATS to the indicated histone peptides, as measured by fluorescence (cr, bu, ac) or NMR (su, hib). Values represent the average of three separate experiments (two for H3K9ac) with error calculated as the SD between the runs. The enhancement in selectivity of Taf14-YEATS to crotonyllysine is comparable to the enhancement in selectivity of other well-recognized epigenetic readers, such as DPFs.[8,11] (c) Representative binding curves used to determine K_d by tryptophan fluorescence. (d) Peptide pull-down assays for Taf14-YEATS using indicated histone H3 peptides. (e) The ribbon diagram of the Taf14-YEATS:H3K9bu complex. Dashed lines and red sphere represent hydrogen bonds and a water molecule, respectively. The YEATS domain is colored lavender and H3K9bu peptide is colored orange. Residues of the YEATS domain involved in the binding of K9bu are labeled. (f) Structural overlay of the acyllysine binding sites in the Taf14-YEATS:H3K9bu (lavender/orange), Taf14-YEATS:H3K9pr (pink) and Taf14-YEATS:H3K9ac[14] (gray) complexes.

Figure 2. Engineering the Taf14-YEATS-based reader of H3K9cr. (a) Surface view of the Taf14-YEATS G82A mutant structure in the apo-state. The side chains of W81, A82 and F62 are shown as green sticks. (b) Structural overlay of the acyllysine binding site in the Taf14-YEATS:H3K9bu (lavender/orange) complex and the apo state of Taf14-YEATS G82A (green). (c) Superimposed ^{1}H,^{15}N HSQC spectra of uniformly ^{15}N-labeled G82A mutant of Taf14-YEATS recorded while the indicated peptides were added stepwise. The spectra are color coded according to the protein:peptide molar ratio. (d) Binding curves used to determine K_d of taf14-YEATS G82A by tryptophan fluorescence. (e) Real-time qPCR analysis of various transcripts in

607 the wild-type strain, *TAF14* delete strain, and *taf14* mutant strains. The mean ± SD are
608 calculated from three biological replicates.
609
610 **Figure 3. Structural basis for recognition of crotonyllysine by Taf14-YEATS G82A.** (a) The
611 ribbon diagram of the Taf14-YEATS G82A:H3K9cr complex. Dashed lines and red sphere
612 represent hydrogen bonds and a water molecule, respectively. (b) Close up view of the H3K9cr-
613 binding site of Taf14-YEATS G82A. Red dashed lines represent short distances indicative of the
614 aromatic-aliphatic-aromatic π stacking interaction. (c) A representative HOMO-8 (see also
615 Supplementary Figure 6).
616
617 **Figure 4. Structural insight into the selectivity of AF9-YEATS.** (a) Alignment of the YEATS
618 domain sequences: absolutely, moderately and weakly conserved residues are colored green,
619 orange and pink, respectively. (b) Binding affinities of AF9-YEATS to indicated histone peptides.
620 Values represent the average of three separate experiments with error calculated as the SD
621 between the runs. (c) Structural overlay of the acyllysine binding sites in the AF9-
622 YEATS:H3K9bu (pink) and AF9-YEATS:H3K9cr[17] (light gray) complexes. Yellow dashed lines
623 represent short distances indicative of the aromatic-amide-aromatic π stacking interaction in
624 AF9-YEATS:H3K9cr[17]. Red dashed lines represent short, less than 4 Å, distances between the
625 crotonyl alkene group and the aromatic residues. (d) Superimposed ^{1}H,^{15}N HSQC spectra of
626 AF9-YEATS, wt and Y78W mutant, recorded in the presence of increasing concentration of
627 H3K9cr peptide. Spectra are color-coded according to the protein:peptide molar ratio. (e)
628 Representative binding curves used to determine K_d of AF9-YEATS Y78W by tryptophan
629 fluorescence. (f) The ribbon diagram of the AF9-YEATS Y78W:H3K9cr complex. Red dashed
630 lines represent short, less than 4 Å, distances between the crotonyl alkene group of H3K9cr and
631 the aromatic residues of the protein.

Figure 5. AF9-YEATS binds DNA. (a) Binding affinities of AF9-YEATS and Taf14-YEATS to indicated histone peptides. Values represent the average of three separate experiments with error calculated as the SD between the runs. (b) Electrostatic potential surface representation of the AF9 YEATS in complex with H3K9cr generated in PyMol (PDB ID PDB 5hjb). Basic residues are labeled. (c) EMSA with 147 bp 601 DNA (1.88 pmol/lane) incubated with increasing amounts of AF9-YEATS. DNA to protein molar ratio is shown below the gel image. (d) Superimposed $^{1}H,^{15}N$ HSQC spectra of uniformly ^{15}N-labeled AF9-YEATS collected upon titration with 601 DNA. The spectra are color coded according to the protein:DNA molar ratio. (e-g) EMSA assays with 1 pmol/lane H3K9cr-NCP (e, g) or unmodified NCP (f) incubated with increasing amounts of WT AF9-YEATS or F59A/Y78A mutant. Band intensities in (c, e-g) were quantified by densitometry using ImageJ.

Figure 6. DNA- and H3K9cr- binding sites in AF9-YEATS do not overlap. (a, b) Analysis of chemical shift perturbations in $^{1}H,^{15}N$ HSQC spectra of AF9 YEATS caused by (a) H3K9cr peptide (1:3 molar ratio) or (b) 601 DNA (1:0.5 molar ratio). P indicates a proline residue. '*' indicates that the residue resonances were unassigned in the apo-state. '-' indicates that the residue resonances were unassigned in the H3K9cr-bound state (BMRB 26060). Dashed line indicates selection cut-off (mean + 3 SD). Residues with CSP above the cut-off value are labeled. (c) Identification of the H3K9cr peptide- and 601 DNA- binding sites. Residues with CSP above the cut-off value in (a) and (b) are mapped onto the surface of AF9-YEATS (PDB 5hjb), colored yellow and orange, respectively, and labeled. Residues with no assignments or prolines are colored light grey. (d) The 60^{th} patch (R61K/K63E/K67E, light pink), 90^{th} patch (K92E/R96E/K97E, light blue) and 130^{th} patch (R133E/K134E/K137E, wheat) mutations are mapped onto the surface of AF9-YEATS. (e-g) EMSA assays with 1 pmol/lane 601 DNA (e, f) or

1 pmol/lane H3K9cr-NCP (g) incubated with increasing amounts of WT AF9-YEATS or RKK mutant. Band intensities were quantified by densitometry using ImageJ.

Figure 7. Bivalent binding of AF9-YEATS is not conserved in Taf14-YEATS. (a) EMSA with 5 pmol/lane 20 bp dsDNA incubated with increasing amounts of AF9-YEATS. (b) Binding curves used to determine K_d for the DNA:AF9-YEATS complex by EMSA. The band of free DNA was used for quantification of the complex formation. Binding constants are obtained from duplicate measurements as mean ± standard error. (c) A schematic of the bivalent interaction of AF9-YEATS with histone H3K9cr and DNA. (d) Alignment of the YEATS domain sequences: absolutely, moderately and weakly conserved residues are colored green, orange and pink, respectively. Positively charged residues in three patches are indicated by blue boxes. The residues of AF9-YEATS mutated in this study are labeled. (e) Electrostatic surface potential of Taf14-YEATS in complex with the H3K9cr peptide. (f) EMSA with 1.88 pmol/lane 601 DNA and increasing concentration of Taf14-YEATS.

Figure 1

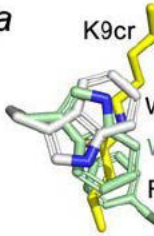

Taf14 YEATS-H3K9cr

b

Binding affinities of Taf14-YEATS

H3 peptide	K_d (μM)
H3K9cr	9 ± 2
H3K9bu	28 ± 2
H3K9su	>700
H3K9hib	NB
H3K9ac	130 ± 8

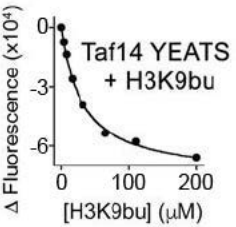

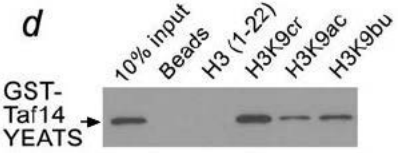

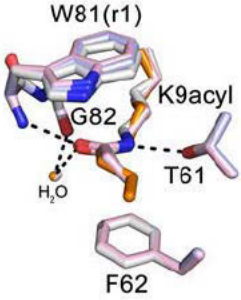

Taf14 YEATS -H3K9bu
-H3K9pr
-H3K9ac

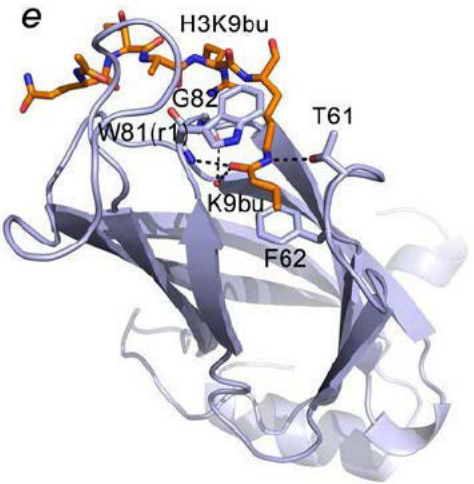

Taf14 YEATS-H3K9bu

Figure 2

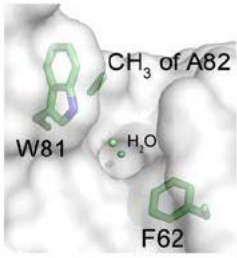
a
CH3 of A82
W81
H2O
F62
Taf14 YEATS G82A
b
W81
W81(r1)
A82
G82
F62
K9bu
Taf14 YEATS G82A
wt Taf14 YEATS-H3K9bu
c
Taf14-YEATS G82A
: H3K9cr
1:0
1:1
1:2
1:5
1:10
8.5
8.0
1H chem. shift (ppm)
Taf14-YEATS G82A
: H3K9ac
1:0
1:1
1:2
1:5
1:10
8.5
8.0
1H chem. shift (ppm)
108
112
15N chem. shift (ppm)
d
Taf14 YEATS G82A
+ H3K9cr
Kd=124±41 μM
0
-4
Δ Fluorescence (x10⁴)
0
250
[H3K9cr] (μM)
e
6.0
4.0
2.0
0.0
Fold change over ACT1
TAF14
taf14Δ
taf14 W81A
taf14 G82A
YBL041
YPR145
YPR158
YLR290
YER145C
YKL150W
YKR039W
YAL017
MRPL10

Figure 3

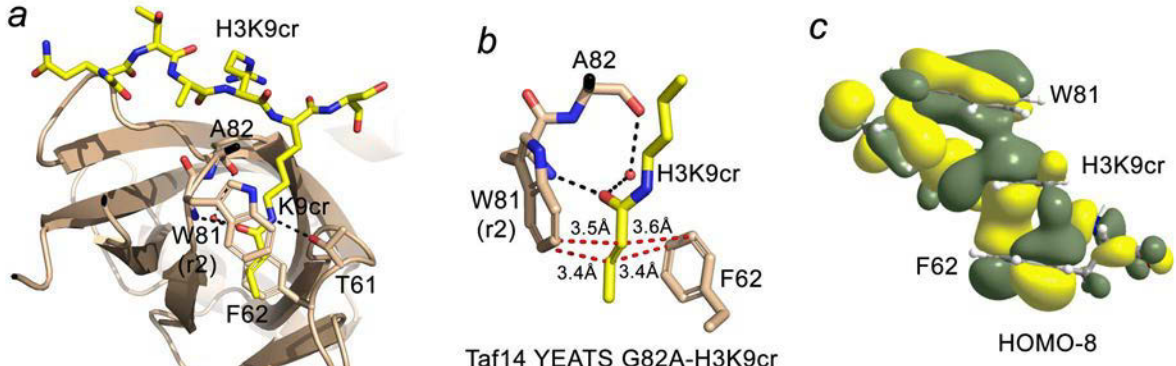
a
H3K9cr
A82
K9cr
W81
(r2)
T61
F62
Taf14 YEATS G82A-H3K9cr
b
A82
H3K9cr
W81
(r2)
3.5Å
3.6Å
3.4Å
3.4Å
F62
Taf14 YEATS G82A-H3K9cr
c
W81
H3K9cr
F62
HOMO-8

Figure 4

b

Binding affinities of AF9 YEATS

AF9 YEATS	H3 peptide	K_d (μM)
WT	H3K9cr	3.7 ± 0.3
WT	H3K9bu	3.9 ± 0.5
WT	H3K9ac	4.3 ± 0.3
Y78W	H3K9cr	2.0 ± 0.3
Y78W	H3K9ac	2.3 ± 0.5

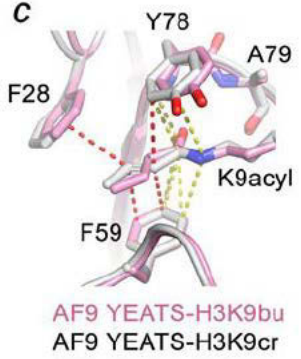

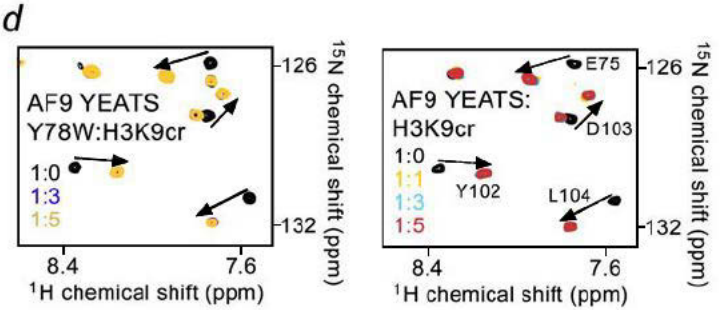

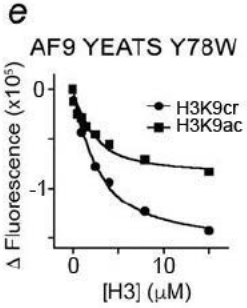

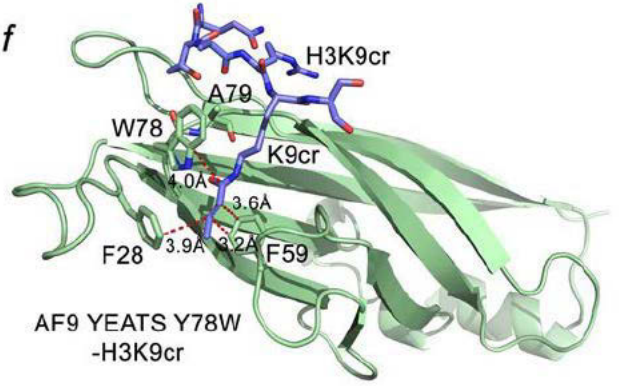

Figure 5

a

YEATS protein	peptide	K_d (μM)
AF9 Y78WA79G	H3K9cr	2.7 ± 0.3
AF9 Y78WA79G	H3K9ac	2.6 ± 0.6
Taf14 W81Y	H3K9cr	9.2 ± 0.9
Taf14 W81Y	H3K9bu	40 ± 1

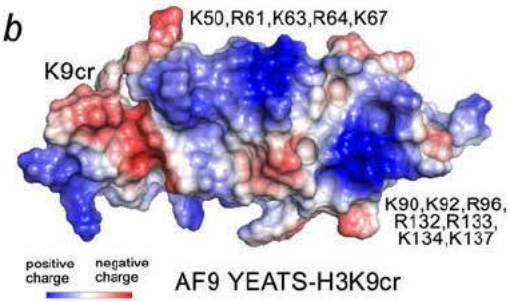

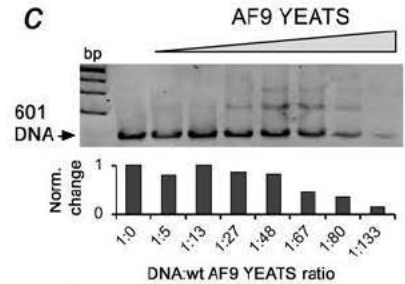

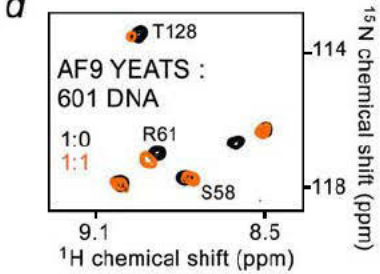

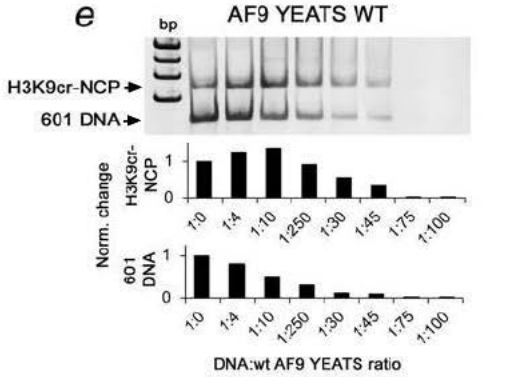

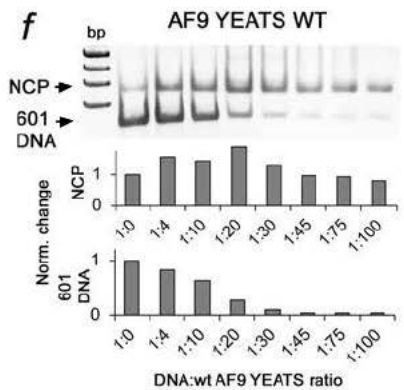

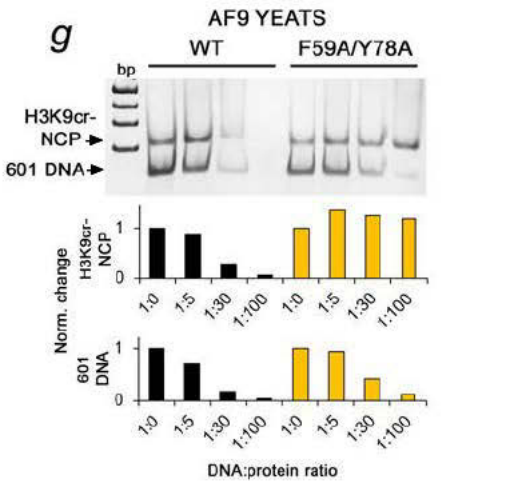

Figure 6

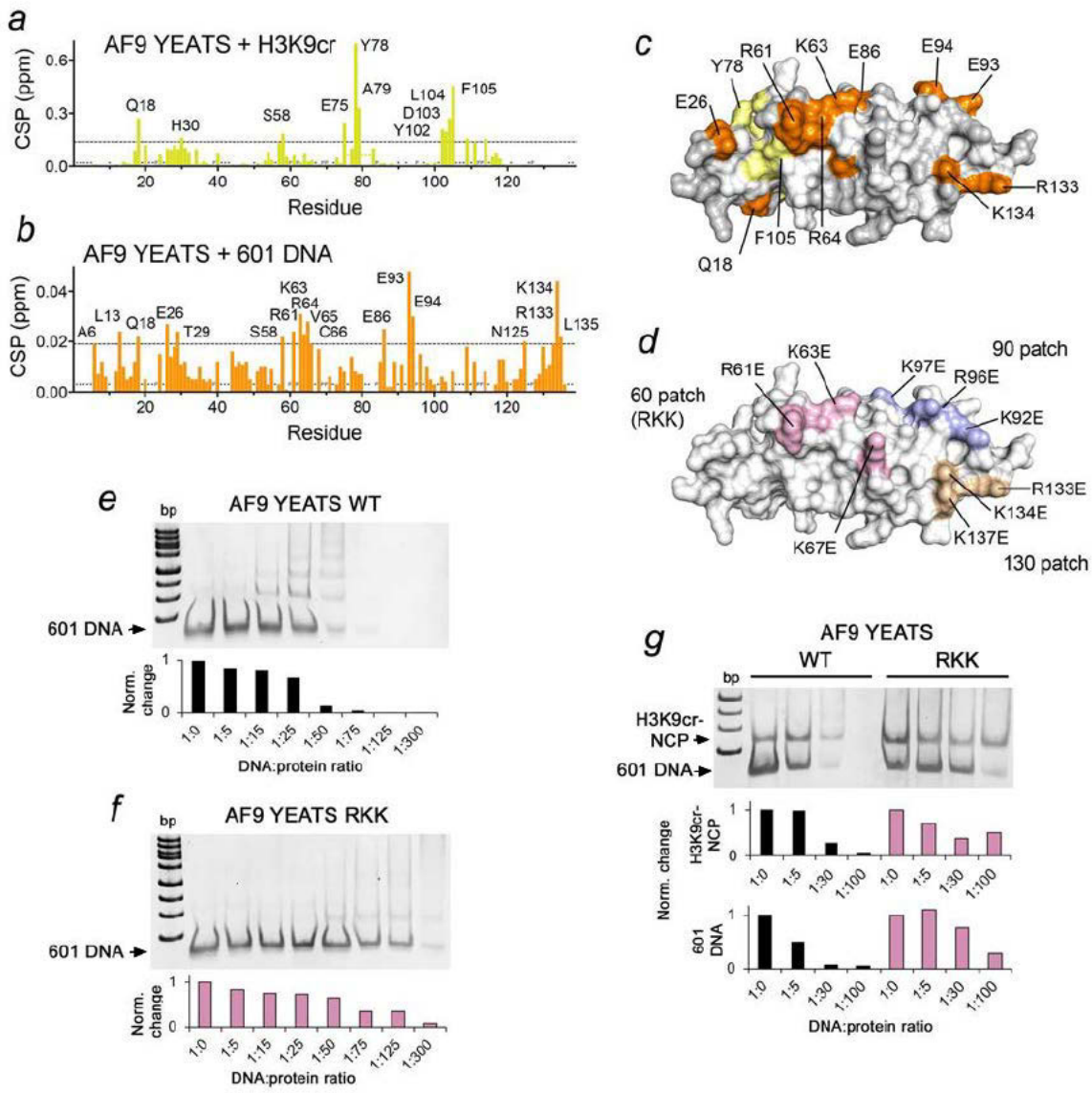
a
AF9 YEATS + H3K9cr
CSP (ppm)
Residue
Q18
H30
S58
E75
Y78
A79
L104
D103
Y102
F105
b
AF9 YEATS + 601 DNA
CSP (ppm)
Residue
A6
L13
Q18
E26
T29
S58
K63
R64
R61
V65
C66
E86
E93
E94
N125
K134
R133
L135
c
R61
K63
E86
E94
E93
Y78
E26
R133
K134
F105
R64
Q18
d
90 patch
R61E
K63E
K97E
R96E
60 patch
(RKK)
K92E
R133E
K134E
K137E
K67E
130 patch
e
AF9 YEATS WT
bp
601 DNA
Norm. change
1:0
1:5
1:15
1:25
1:50
1:75
1:125
1:300
DNA:protein ratio
f
AF9 YEATS RKK
bp
601 DNA
Norm. change
1:0
1:5
1:15
1:25
1:50
1:75
1:125
1:300
DNA:protein ratio
g
AF9 YEATS
WT
RKK
bp
H3K9cr-NCP
601 DNA
Norm. change
H3K9cr-NCP
601 DNA
1:0
1:5
1:30
1:100
DNA:protein ratio

Figure 7

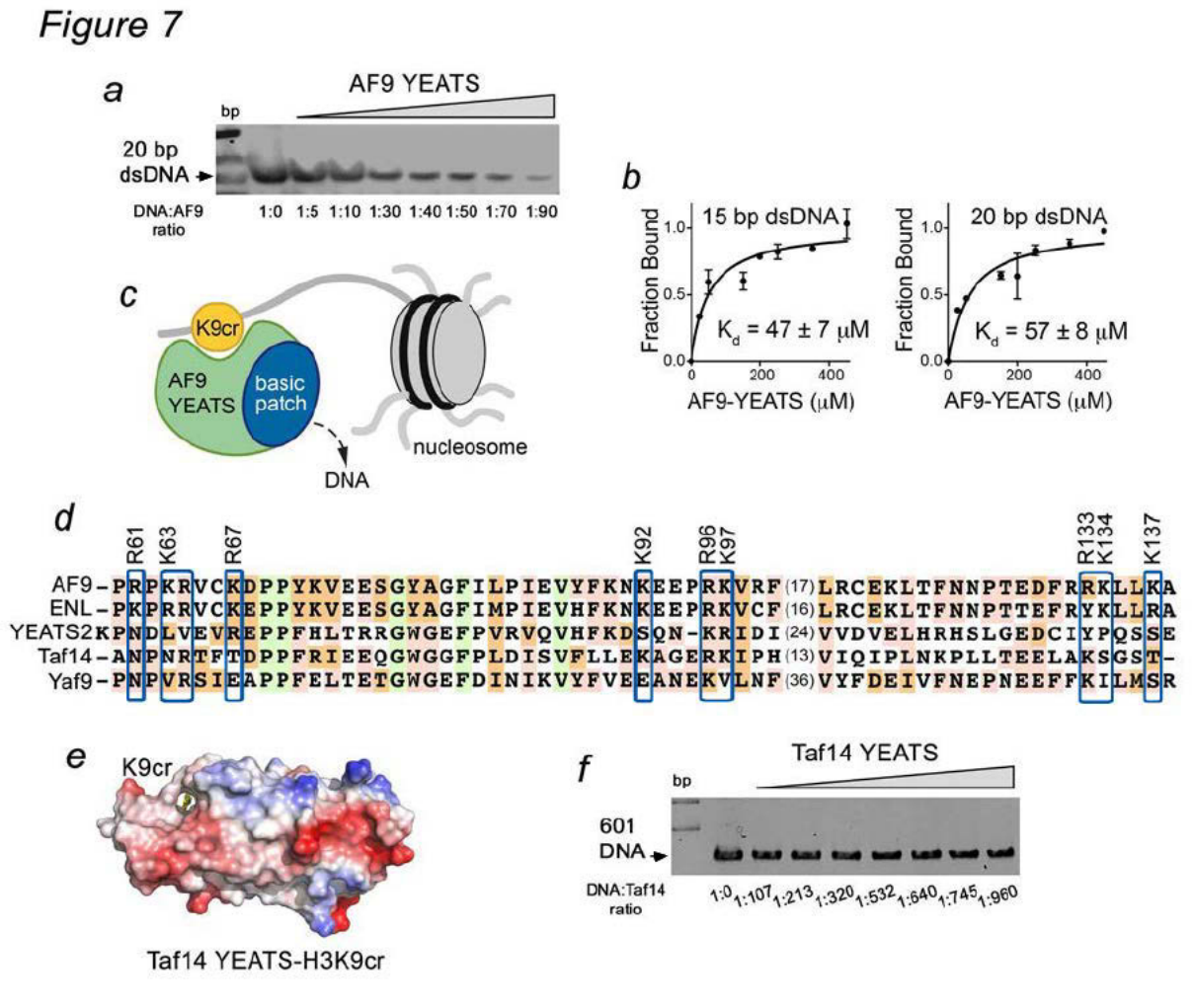
a
AF9 YEATS
bp
20 bp
dsDNA
DNA:AF9
ratio
1:0 1:5 1:10 1:30 1:40 1:50 1:70 1:90
b
15 bp dsDNA
20 bp dsDNA
Fraction Bound
K_d = 47 ± 7 μM
K_d = 57 ± 8 μM
AF9-YEATS (μM)
c
K9cr
AF9
YEATS
basic
patch
nucleosome
DNA
d
R61
K63
R67
K92
R96
K97
R133
K134
K137
AF9 -PRPKRVCKDPPYKVEESGYAGFILPIEVYFKNKEEPRKVRF (17) LRCEKLTFNNPTEDFRRKLLKA
ENL -PKPRRVCKEPPYKVEESGYAGFIMPIEVHFKNKEEPRKVCF (16) LRCEKLTFNNPTTEFRYKLLRA
YEATS2KPNDLVEVREPPFHLTRRGWGEFPVRVQVHFKDSQN-KRIDI (24) VVDVELHRHSLGEDCIYPQSSE
Taf14 -ANPNRTFTDPPFRIEEQGWGGFPLDISVFLLEKAGERKIPH (13) VIQIPLNKPLLTEELAKSGST-
Yaf9 -PNPVRSIEAPPFELTETGWGEFDINIKVYFVEEANEKVLNF (36) VYFDEIVFNEPNEEFFKILMSR
e
K9cr
Taf14 YEATS-H3K9cr
f
Taf14 YEATS
bp
601
DNA
DNA:Taf14
ratio
1:0 1:107 1:213 1:320 1:532 1:640 1:745 1:960